PAPER • OPEN ACCESS

Performance and properties of the first plasmas of Wendelstein 7-X

To cite this article: T Klinger *et al* 2017 *Plasma Phys. Control. Fusion* **59** 014018

View the article online for updates and enhancements.

Performance and properties of the first plasmas of Wendelstein 7-X

T Klinger[1], A Alonso[2], S Bozhenkov[1], R Burhenn[1], A Dinklage[1], G Fuchert[1], J Geiger[1], O Grulke[1], A Langenberg[1], M Hirsch[1], G Kocsis[3], J Knauer[1], A Krämer-Flecken[4], H Laqua[1], S Lazerson[5], M Landreman[6], H Maaßberg[1], S Marsen[1], M Otte[1], N Pablant[5], E Pasch[1], K Rahbarnia[1], T Stange[1], T Szepesi[3], H Thomsen[1], P Traverso[7], J L Velasco[2], T Wauters[8], G Weir[1], T Windisch[1] and The Wendelstein 7-X Team[9]

[1] Max-Planck Institute for Plasma Physics, Greifswald, Germany
[2] Laboratorio Nacional de Fusión, CIEMAT, Madrid, Spain
[3] Wigner Research Center for Physics, Budapest, Hungary
[4] Research Center Jülich, Jülich, Germany
[5] Princeton Plasma Physics Laboratory, Princeton, NJ, USA
[6] University of Maryland, Maryland, MD, USA
[7] Auburn University, Auburn, AL, USA
[8] LPP-ERM/KMS, Brussels, Belgium

E-mail: thomas.klinger@ipp.mpg.de

CrossMark

Abstract

The optimized, superconducting stellarator Wendelstein 7-X went into operation and delivered first measurement data after 15 years of construction and one year commissioning. Errors in the magnet assembly were confirmed to be small. Plasma operation was started with 5 MW electron cyclotron resonance heating (ECRH) power and five inboard limiters. Core plasma values of $T_e > 8$ keV, $T_i > 2$ keV at line-integrated densities $n \approx 3 \cdot 10^{19}$ m^{-2} were achieved, exceeding the original expectations by about a factor of two. Indications for a core-electron-root were found. The energy confinement times are in line with the international stellarator scaling, despite unfavourable wall conditions, i.e. large areas of metal surfaces and particle sources from the limiter close to the plasma volume. Well controlled shorter hydrogen discharges at higher power (4 MW ECRH power for 1 s) and longer discharges at lower power (0.7 MW ECRH power for 6 s) could be routinely established after proper wall conditioning. The fairly large set of diagnostic systems running in the end of the 10 weeks operation campaign provided first insights into expected and unexpected physics of optimized stellarators.

Keywords: stellarator, optimization, plasma performance, central electron root

(Some figures may appear in colour only in the online journal)

1. Introduction

The large superconducting stellarator device Wendelstein 7-X has created its first plasma on the 10th of December 2015 after more than 15 years of construction. Plasma volume, heating power density, and wall conditions have been chosen to provide relevant data for extrapolation to a potential HELIAS-type fusion reactor [1]. This line is based on the use of modular, non-planar coils to shape the geometry of the magnetic field in a favourable way. The goal is to find an

[9] Author list Nuclear Fusion Vol. 53 No. 12 Article 126001 (2013)

optimized magnetic field geometry that complies with the following seven requirements [2]:

 (i) Nested vacuum field magnetic flux surfaces with sufficiently small relative thickness of the magnetic islands must be established.
 (ii) At finite $\langle \beta \rangle \leqslant 4\%$ the equilibrium properties are favourable with minimized Shafranov shift and small changes of size and location of the outermost island structures.
(iii) Resistive magnetohydrodynamic (MHD) balooning and interchange stability must be ensured at sufficiently high $\langle \beta \rangle$.
(iv) The effective ripple ϵ_{eff} is minimized to reduce the neoclassical transport in the $1/\nu$ regime.
 (v) The equilibrium currents (in particular bootstrap I_{BS} and Pfirsch–Schlüter I_{PS}) are reduced to minimize undesired changes of the edge rotational transform $\dotplus(a)$, especially at high $\langle \beta \rangle$.
(vi) The plasma equilibrium at $\langle \beta \rangle \approx 4\%$ aims at beneficial fast-particle confinement with a sufficiently small prompt loss fraction f_{α} (esp. in the long-mean-free path regime).
(vii) The engineering feasibility of the non-planar coils requires both sufficiently large curvature radii R_{c} in the coil contours and sufficiently large distance from the plasma first wall ΔW.

This path to stellarator optimization was pursued by using coupled numerical codes for MHD equilibrium and stability, neoclassical transport, drift orbits, and divertor loads. Non-axisymmetric shaping of the magnetic field is nowadays of significant interest in the general physics of magnetic confinement, far beyond the stellarator concept alone [3].

The stellarator Wendelstein 7-X was designed on the basis of the above described physics optimization procedure. Optimization is always a compromise and there are uncertainties in the numerical codes. It is thus a major goal of Wendelstein 7-X to demonstrate that magnetic field optimization along the above described line results in significantly better plasma performance combined with properties required for a fusion reactor, e.g. fast particle confinement and divertor feasibility. Figure 1 shows a design drawing of the Wendelstein 7-X device. The 50 modular non-planar and the 20 planar superconducting NbTi coils are the key components for the steady-state operation of the device. Manufacturing, test and assembly of the coils took in total eight years and considerable efforts were necessary due to extremely high quality and reliability requirements [4]. The high number of device components and the resulting space restrictions have resulted in demanding requirements on design engineering, component manufacturing and assembly in the cryostat, i.e. the volume between the three-dimensionally shaped plasma vessel and the outer vessel. The 254 ports (with 120 variants) and the more than 500 openings in the outer vessel have added further to the overall engineering complexity of the device. To tackle this complexity, it became necessary to use (and further develop) most advanced tools on design engineering, metrology, tooling, and manufacturing—everything to deal with fully 3D geometry.
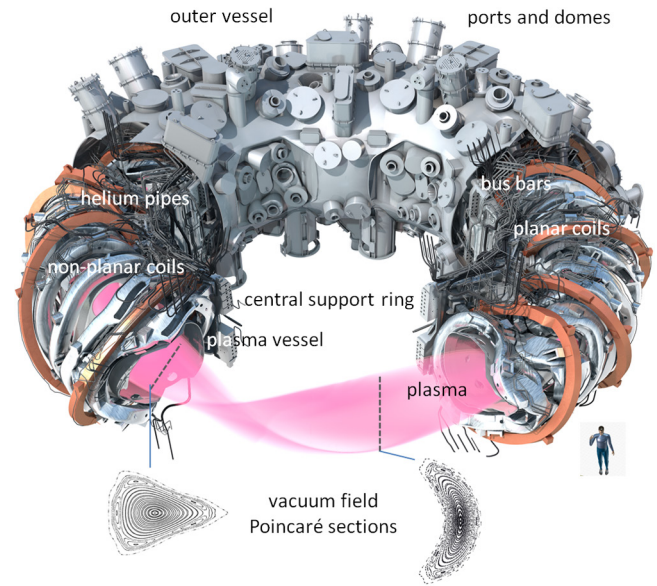

Figure 1. Schematic diagram of the superconducting stellarator Wendelstein 7-X. The last closed magnetic flux surface is indicated in magenta. The plasma vessel is shaped according to the magnetic field geometry. The 50 non-planar coils have an aluminum foil plated steel casing, the 20 planar coils a copper plated steel casing. The non-planar and the planar coils of each type are connected in series via superconducting bus bars. Coils, coil casings and the central support ring are supplied with liquid helium by means of a pipe system. The magnet system is operated in the evacuated cryostat volume between the plasma vessel and the outer vessel.

Table 1. Major parameters of the stellarator Wendelstein 7-X.

Quantity	Min	Max	Ext	Unit
Plasma volume		30		m^3
Major radius		5.5		m
Minor radius		0.5		m
Magnetic induction on axis[a]	0	2.5	3.0	T
Rotational transform	5/6	5/4		2π
Electron cyclotron resonance heating power[a]	0.6	4.3	10	MW
Heating energy[a]	0.05	4	18 000	MJ
Pulse length[a]	0.05	6	1800	s

[a] The parameters represent the initial setup for the first operaion phase and are subject to substantial increases for later operation. Their design values are listed in the column 'ext'.

The project Wendelstein 7-X was initiated to explore the reactor potential of optimized HELIAS-type stellarators and to adress critical plasma physics issues. At the same time, during design, development and assembly of Wendelstein 7-X, important know-how in engineering and technology was acquired. The mission of the project Wendelstein 7-X is to bring stellarators to maturity and to assess the reactor capabilities of the HELIAS line [5]. It can be summarized in four different points:

- Constructability with the required precision, mechanical stability, and reliability,
- Stable operation of integrated plasma scenarios at reactor-relevant $nT\tau_E$ and $\langle \beta \rangle$,
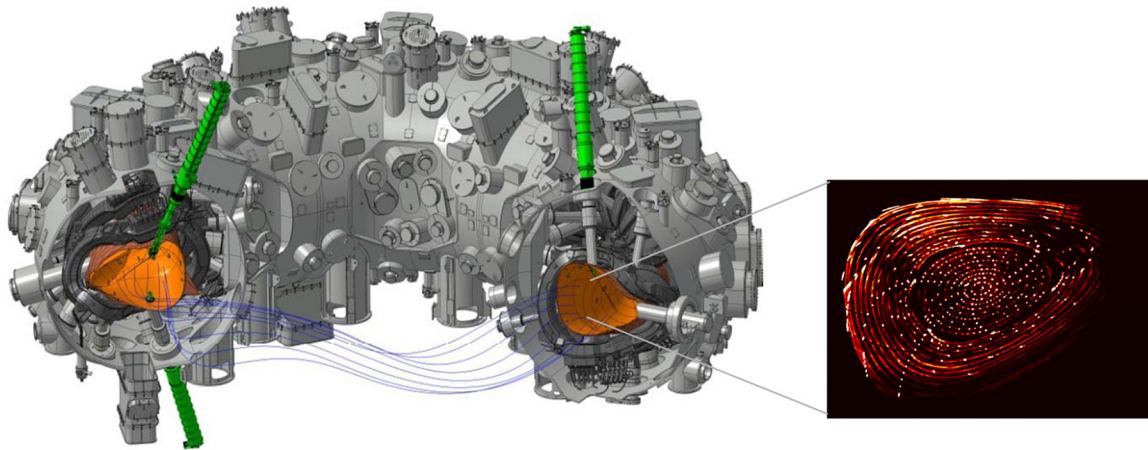
Figure 2. Flux surface measurement with electron beam [9]. One radial manipulator (green) is used to position the electron gun, another for scanning the cross section of the magnetic field with a fluorescent rod. The fluorescence light is recorded with a video camera and point-by-point the magnetic flux surface is reconstructed (inset figure on the right).

- Long-pulse island divertor operation with high recycling conditions and detachment,
- Fully integrated steady-state operation scenarios at 10 MW heating power.

The first point was already accomplished with the successful start of Wendelstein 7-X (see below). The other points will be subject to a dedicated research program based on a staged approach: the first stage is plasma operation with five inboard limiters and metallic wall. The second stage will have installed ten inertially cooled island divertor modules and graphite elements on highly loaded wall segments. The third stage will have the the same geometry of plasma facing components but with pressurized water cooling of the divertor and all wall elements. The maximum allowable heating energy is planned to be increased step-wise from 4 MJ to 80 MJ to 18 GJ (the latter at 1800 s pulse length). Especially the last stage requires operation experience to mitigate technical risk and discharge scenarios that are consistent with the operation limits of the divertor. The development of these scenarios will be made during the second stage with the inertially cooled divertor: here the target plates consist of simple graphite elements that are fairly robust against thermal overloads. A different situation arises with the pressure water cooled divertor, where the target plates are based on carbon fibre reinforced carbon (CFC) elements that are electron-beam welded to a copper-chrome zirconium heat sink. The interface between the CFC and the heat sink is prone to delamination if the maximum heat flux of 10 MW m^{-2} is exceeded. Consequently, only well defined and controlled plasma scenarios can be used.

The main parameters of Wendelstein 7-X for the initial first stage operation (10 weeks duration) are compiled in table 1. The heating power was restricted by the available number of gyrotons and the heating energy by the maximum allowable limiter loads.

2. Device commissioning and flux surfaces

Owing to the high complexity of Wendelstein 7-X, it was necessary to establish strict procedures for the device commissioning [6]. The consecutive commissioning steps were continuously supervised by a dedicated group of experts. Proper documentation and systematic quality assurance have been indispensable. The six main device commissioning steps are the following:

- Pump-down of the cryostat to high vacuum conditions,
- Cool-down of the magnet system to 3.4 K,
- Test of the normal conducting trim coils,
- Pump-down of the plasma vessel to ultra high vacuum conditions,
- Ramp-up of the superconducting coils to 2.5 T on axis,
- Plasma preparation, i.e. plasma vessel baking, wall conditioning, gas inlet test etc.

An additional commissioning step was the measurement of magnetic flux surfaces. The vacuum magnetic field of a stellarator has confinement properties and magnetic flux surfaces can be made visible by an electron beam mapping method (figure 2): an electron gun attached to a radial manipulator is scanned over the cross section of the torus and injects an electron beam along the magnetic field line. A fluorescent rod is moved over a cross section at a distant toroidal location. If the rod intersects the magnetic surface on which the beam is propagating, visible light is emitted. This light is recorded step-by-step with a video camera and eventually the Poincaré section of the magnetic field is obtained (see figure 2 right inset figure). The direct measurement of the magnetic flux surfaces verifies the first of the optimization criteria (see above), i.e. well nested magnetic flux surfaces and minimization of low-order intrinsic magnetic field perturbations; for a more comprehensive discussion we refer the reader to [7]. The quality of the magnetic field is not only given by the actual optimization procedure but also by the manufacturing precision of the coil winding packs and the assembly of the coils within a tolerance of ±1.5 mm. Beyond the existence of flux-surfaces, the magnetic field of Wendelstein 7-X is designed to have natural magnetic islands at the edge. An example of a direct measurement of magnetic islands is shown in figure 3 [8, 9].
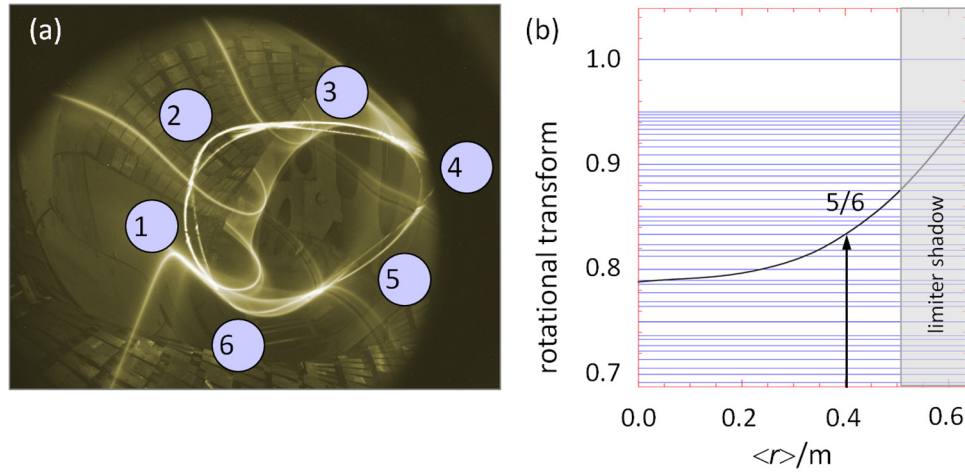
Figure 3. (a) Toroidal view into the plasma vessel with a Poincaré mapping of magnetic islands at the $\iota = n/m = 5/6$ resonance, occuring at $r_{eff} = 40$ cm. Clearly seen is the chain of magnetic islands labeled from 1 … 6. A thin background gas in the chamber creates a visualization of the field lines at the X-points of the island chain. (b) Radial ι-profile with resonances indicated by blue lines. The radial position of the $n/m = 5/6$ resonance is marked by an arrow. The limiter shadow is indicated by the gray shaded area.
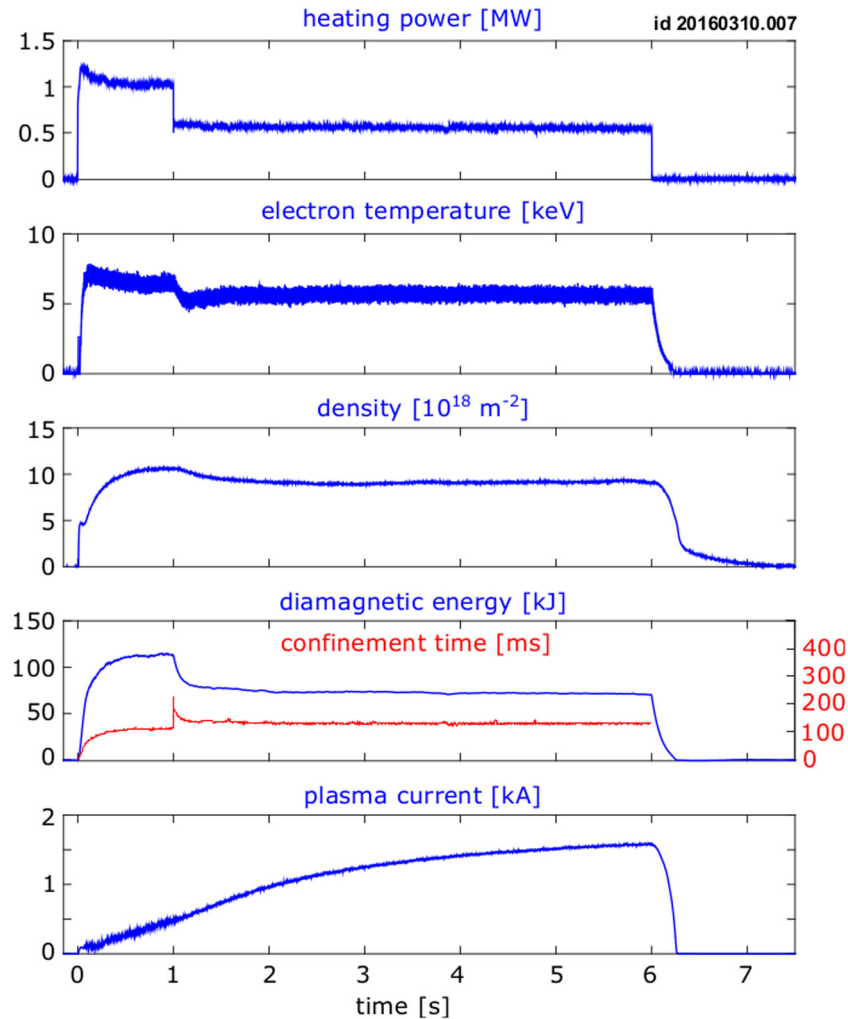

Figure 4. Time evolution of main plasma parameters during a long hydrogen discharge. Shown are (from top to bottom) the ECRH power, the central electron temperature, the line-integrated plasma density, the diamagnetic energy (left label), the energy confinement time (red curve, right label), and the toroidal plasma current.

Figure 5. Time evolution of main plasma parameters during a hydrogen discharge with higher ECRH power. Shown are (from top to bottom) the ECRH power, the central electron temperature, the line-integrated plasma density, the diamagnetic energy (left label), the energy confinement time (red curve, right label), and the toroidal plasma current.
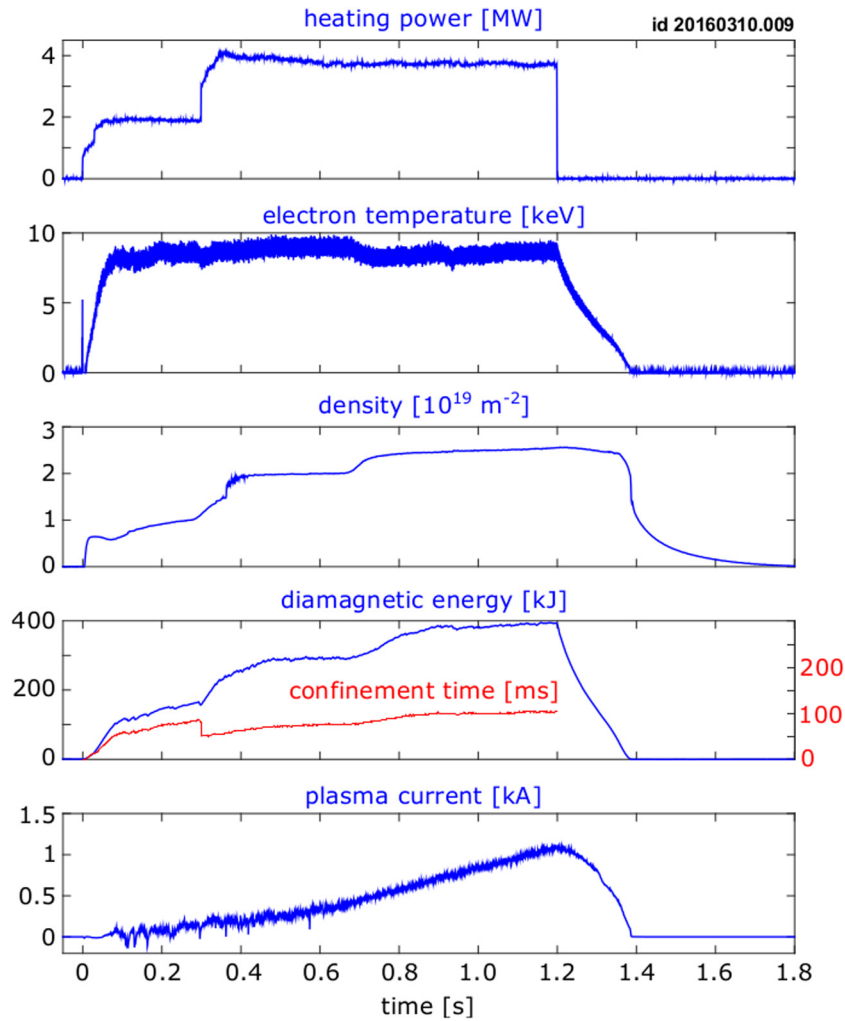
Since magnetic islands occur at resonant magnetic surfaces (here at $\iota = n/m = 5/6$ within the last-closed flux surface) their size and position are extremely sensitive to deviations of the coil current paths from their calculated contours. It turns out that the location of the island chain is almost exactly at the expected position if the elastic deformation of the coil windings in their steel casings is taken into account [7]. This deformation is the natural consequence of their non-planar shape which leads in operation to $\vec{j} \times \vec{B}$ force driven shear stress [10]. This result clearly shows that the assembly of the magnet system of Wendelstein 7-X was successfully achieved within the tolerance requirements, despite extreme demands on machining, fitting and welding [11].

3. Wall conditioning and plasma operation

The available heating system was electron cyclotron resonance heating (ECRH) in X- or O-mode with six gytrotrons and a total of 4.3 MW maximum heating power. The wave frequency is 140 GHz with a resonance at the 2.5 T contour. Further details can be found in [12, 13]. The first plasmas

in Wendelstein 7-X were generated in helium on the 10th of December 2015. Mainly due to the unfavourable wall conditions, the pulse length was limited by strong plasma radiation to ≈ 50 ms. At line-integrated density $\bar{n} \approx 2 \cdot 10^{19}$ m^{-2} central electron and ion temperatures of $T_e(0) = 1$ keV and $T_i(0) < 1$ keV were achieved. With reduced outgassing from the walls and the limiter elements, the pulse length could be rapidly prolonged to ≈ 500 ms with temperatures $T_e(0) = 8$ keV and $T_i(0) = 2$ keV, respectively, at plasma densities of $\bar{n} = 3 \cdot 10^{19}$ m^{-2}. These values were already about a factor two beyond the initial expectations that were based on 1D transport calculations with rather conservative parameter assumptions [14]. Glow discharge wall conditioning was at that time not yet available and wall conditioning was made with a sequence of short low-power ECR heating pulses. After switching to hydrogen as filling gas and with the availablity of the glow discharge system the plasma performance has drastically improved [15]: the first hydrogen plasma on the 3rd of February 2016 was 250 ms long with temperatures $T_e(0) = 7$ keV and $T_i(0) = 1.2$ keV at plasma density $\bar{n} = 3 \cdot 10^{19}$ m^{-2}. After 20–40 min glow discharge conditioning before the ramp-up of the magnetic field (note that
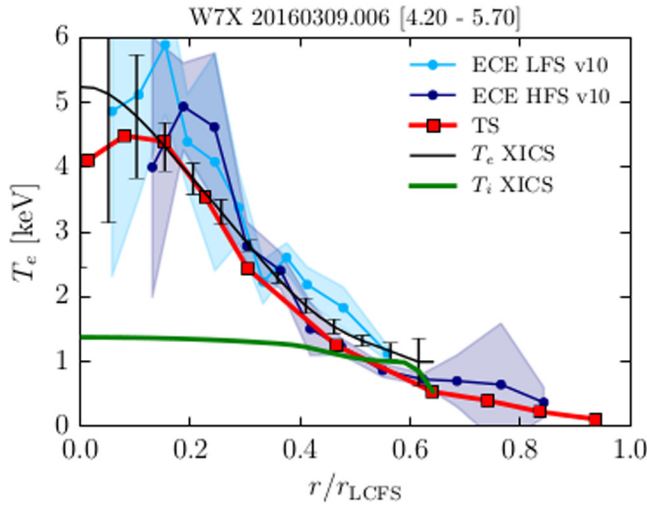
Figure 6. Radial electron and ion temperature profiles measured with electron cyclotron emission (ECE on the high field and the low field side), Thomson scattering (TS), and with the x-ray imaging crystal spectrometer (XICS).
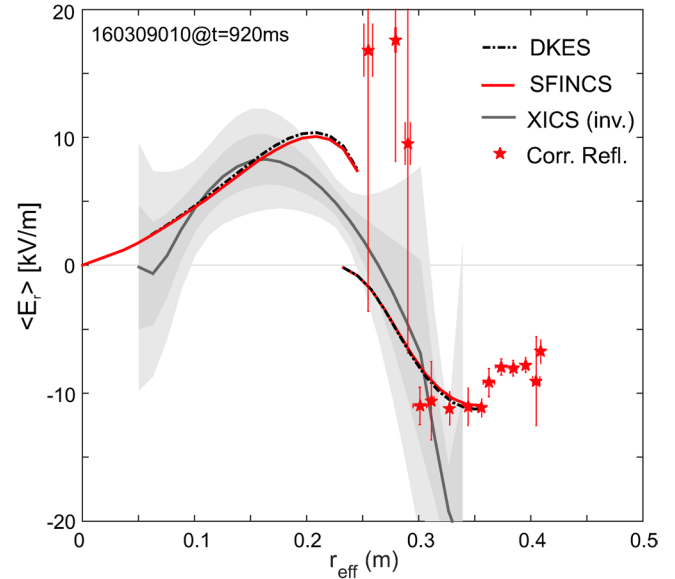

Figure 7. Measurement of the radial electric field by means of correlation reflectometry (red stars) and line-integrated x-ray spectroscopic data (inverted profile plotted in black). The uncertainty is indicated by error bars for the reflectometry data and by gray shades for the x-ray data. The radial electric field changes sign at $r_{eff} = 0.25$ and 0.3 m. Also shown are neoclassical transport calculations using the DKES code (blue dashed–dotted line) and the SFINCS code (red line).
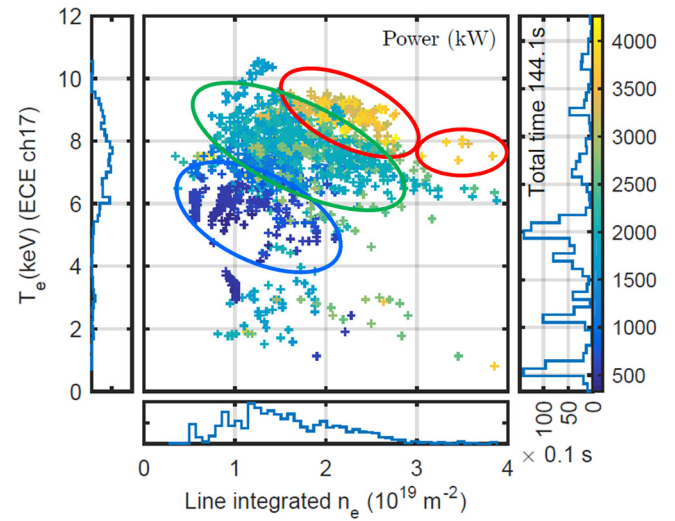

Figure 8. Overview plot of the hydrogen discharges of Wendelstein 7-X. Each point in the T_e-$\bar{n}_e$-plane corresponds to a 100 ms stable plasma segment. The colour code indicates the ECRH power. The two histograms on the left and on the bottom of the diagram indicate the number of points. The histogram on the right hand side indicates the number of 100 ms segments at the respective ECRH power. The three ellipses mark the low-power long-discharge regime (blue), the higher-power short-discharge regime (red) and the intermediate regime (green). The higher-power discharges ususally correspond to shorter plasma durations and vice versa.

the magnetic field is usually kept up during the entire experiment day) stationary plasma density was achieved and long discharge durations became accessible. Outgassing turned out to be a major impurity source which and proper wall conditioning was decisive for plasma performance and duration. A more complete discussion including model considerations is found in [15]. As a consequence, the main impurities observed in the plasma were oxygen and carbon, followed by traces of sulfur and chlorine [16] and surprisingly little indication for copper and iron.

Figure 4 shows the main plasma parameter evolution during a 6 s discharge in hydrogen at relatively low ECRH power. Note that the total injected heating energy was restricted to 4 MJ to avoid overheating of wall elements and yet unprotected diagnostics. For plasma startup, 1 MW ECRH power is maintained for ~ 1 s and then lowered to 0.6 MW. One obtains quite reasonable plasma parameters with $T_e(0) = 5$ keV and $\bar{n} = 1 \cdot 10^{19}$ m^{-2}. The plasma diamagnetic energy is measured with a diamagnetic loop located at a triangular-shaped cross section of the torus [17]. The diamagnetic energy is $E_{dia} = 100$ kJ during the first 1 s of heating and drops to $E_{dia} = 60$ kJ for the remaining discharge. Remarkable is the bootstrap current, measured with Rogowski coils [17]: it rises during the first 2 s at a constant rate to about 1000 A, then at a lower rate to its peak value of 1800 A. Saturation is not yet reached as expected because of the combined effect of the skin time and the L/R-time being > 10 s. The magnitude of the bootstrap current is within the expected range while the details of its temporal evolution are still under investigation.

A typical hydrogen discharge at higher heating power is shown in figure 5. After the initial plasma start-up the ECRH power is increased to 4.3 MW. The electron temperature is close to 10 keV. At $t = 600$ ms a hydrogen gas puff results in an increase of the plasma density, a slight drop in the electron temperature, and in a rise of the diamagnetic energy to $E_{dia} = 400$ kJ. The bootstrap current is constantly rising to about 1000 A. The fraction of radiated power is $\approx 30\%$ and

the energy confinement time is determined to be $\tau_E \approx 100$ ms (under slightly different conditions $\tau_E \approx 150$ ms was reached [14]). The latter value is in line with the ISS04 scaling [18], which is already an encouraging result, taking into account unwanted energy loss channels, e.g. charge exchange collisions

with neutrals in the scrape-off-layer. Better scaling behaviour is expected after the installation of the island divertor and wall coverage with graphite tiles.

An example of radial profiles of the electron and the ion temperature in a hydrogen plasma is shown in figure 6. The measurements obtained with electron cyclotron emission, Thomson scattering, and fitting argon imurity spectral lines obtained with an x-ray imaging (crystal) spectrometer (XICS) [20] are in rather good agreement and clearly show a peaked electron temperature profile with $T_e > T_i$ everywhere in the plasma volume. (For the inverse electron temperature gradient length we find values in the range $L_{T_e}^{-1} = 6 \dots 8$ m^{-1}.) The ion temperature profile is quite flat in the centre and approaches T_e at $r/r_{LCFS} > 0.6$. The peaked electron temperature profile indicates improved core energy confinement for the electrons. The so-called 'core electron-root confinement' [19] requires a positive radial electric field E_r in the core region, sufficiently large to strongly reduce neoclassical transport coefficients of the electrons.

A change of the sign in the radial electric field was indeed observed as shown in figure 7. The radial electric field was measured with two different methods: firstly, with correlation reflectometry using five poloidally separated antennae 24 … 40 GHz in O-mode polarization, secondly by x-ray imaging spectroscopy (XICS, see above). Both diagnostics reveal a change in the sign of E_r at $r_{eff} = 0.25 \dots 0.3$ m with a positive electric field in the plasma core. The large velocity shear in the transition region leads to a relatively high uncertainty in the reflectometry data, probably owing to coherency loss. This trend is confirmed by respective neoclassical transport calculations using the DKES code [21] with input parameters and profiles from the present plasma discharge. Another comparison using the new SFINCS code [22] is in agreement with the DKES findings and further supports the experimental observation. It can be concluded that in the plasma core ($r/r_{eff} < 0.4$) we have electron-root confinement whereas further outside ion-root confinement conditions prevail.

An overview plot of the Wendelstein 7-X hydrogen discharges is shown in figure 8. All discharges (stable with at least 100 ms duration) are ordered in a plane with the electron temperature T_e as one axis and the the line-integrated density $\bar{n}_e$ the other. The color code of the markers is the ECRH power. There are three main regimes, the low-power long-discharge regime (blue ellipse, see figure 4), the higher-power regime (red ellipses, see figure 5) and an intermediate regime (green ellipse) at about 2 MW ECRH power used for a large variety of experiments. The majority of the discharges can be found within these three regimes. A few outliers are due to bad wall conditions or technical problems. Generally speaking, the plasma operation turned out to be surprisingly reliable and during the 10 weeks of operation about 1000 experiments could be conducted. The detailed data analysis and the comparison with modelling calculations are underway and the main scientific topics under investigation are the following: the scrape-off layer is investigated to prepare island divertor operation [23–25], visible light emission and the formation

of plasma filaments is studied with fast-framing cameras [26, 27], the perturbation of magnetic flux surfaces with trim coils and its impact on limiter heat loads is studied [25, 28], by means of profile data, heat transport and power balance analysis is performed [17, 29–34], the radial electric field and its role for electron- and ion-root confinement is investigated [14, 20], first impurity transport studies are made based on plasma radiation [16], and a variety of electron cyclotron heating scenarios and central electron cyclotron current drive is investigated [13].

4. Summary

The inital hydrogen plasmas of Wendelstein 7-X have proven to be robust and well controllable if a sufficient conditioning of the metal wall and the inboard limiters was performed. Glow discharge wall conditioning was most effective, though conditioning shots with ECRH also have resulted in significant improvement. The main pulse length limitation is due to radiation collapse. Under good conditions, after glow discharge conditioning or ECRH wall conditioning pulses, stable and reproducible discharges could be achieved from low ECRH power (0.6 MW with discharge duration up to 6 s to higher ECRH power (4.3 MW with discharge duration of 1 s). There is strong evidence for central electron-root confinement, with peaked electron temperature profiles and a positive radial electric field in the core region. The energy confinement time is in line with the ISS04 scaling. Better performance is expected after the island divertor has been installed and the majority of the wall is covered with graphite tiles.

References

[1] Nührenberg J and Zille R 1986 *Phys. Lett.* A **114** 129
[2] Grieger G *et al* 1992 *Phys. Fluids* B **4** 2081
[3] Boozer A 2009 *Phys. Plasmas* **16** 058102
[4] Wegener L *et al* 2012 *IEEE Trans. Appl. Supercond.* **22** 4201004
[5] Warmer F *et al* 2016 *Plasma Phys. Control. Fusion* **58** 074006
[6] Bosch H-S *et al* 2015 *Fusion Eng. Des.* **96–7** 22
[7] Lazerson S *et al* 2016 *Nucl. Fusion* **56** 106005
[8] Pedersen T S *et al* 2016 *Nat. Commun.* submitted
[9] Otte M *et al* 2016 *Plasma Phys. Control. Fusion* **58** 064003
[10] Andreeva T *et al* 2015 *Nucl. Fusion* **55** 063025
[11] Bräuer T, Klinger T and Bosch H-S 2011 *IEEE Trans. Plasma Sci.* **40** 577
[12] Bosch H S *et al* 2010 *IEEE Trans. Plasma Sci.* **38** 265
[13] Marsen S *et al* 2016 *ECA* **40A** P4.002
[14] Dinklage A *et al* 2016 *ECA* **40A** O2.107
[15] Wauters T *et al* 2016 *ECA* **40A** P2.052
[16] Zhang D *et al* 2016 *ECA* **40A** P4.015

[17] Rahbarnia K *et al* 2016 *ECA* **40A** P4.011
[18] Yamada H *et al* 2005 *Nucl. Fusion* **45** 1684
[19] Yokoyama M *et al* 2007 *Nucl. Fusion* **47** 1213
[20] Pablant N *et al* 2016 *ECA* **40A** P4.013
[21] Hirshman P *et al* 1986 *Phys. Fluids* **29** 2951
[22] Landreman M *et al* 2014 *Phys. Plasmas* **21** 042503
[23] König R *et al* 2016 *Plasma Phys. Control. Fusion* submitted
[24] Drews P *et al* 2016 *ECA* **40A** P4.025
[25] Niemann H *et al* 2016 *ECA* **40A** P4.005

[26] Kocsis G *et al* 2016 *ECA* **40A** P4.003
[27] Szepesi T *et al* 2016 *ECA* **40A** P4.004
[28] Otte M *et al* 2016 *ECA* **40A** O2.105
[29] Bozhenkov S *et al* 2016 *ECA* **40A** O2.106
[30] Pasch E *et al* 2016 *ECA* **40A** P4.016
[31] Knauer J *et al* 2016 *ECA* **40A** P4.017
[32] Höfel U *et al* 2016 *ECA* **40A** P4.008
[33] Hirsch M *et al* 2016 *ECA* **40A** P4.007
[34] Langenberg A *et al* 2016 *ECA* **40A** P4.014